Chemistry – A European Journal

ChemEurJ

Chemistry Europe
European Chemical Societies Publishing

RESEARCH ARTICLE OPEN ACCESS

A High Energy Barrier Dy^{III}_2 Single-Molecule Magnet Supported by a Bulky, Anionic N–O Bridging Ligand

Alexandros S. Armenis[1] | Concepción Molina-Jirón[2,3,4] | Konstantinos N. Pantelis[1] | Wolfgang Wernsdorfer[2,5] | Mario Ruben[2,6] | Eufemio Moreno-Pineda[2,4,7] | Theocharis C. Stamatatos[1]

[1]Department of Chemistry, University of Patras, Patras, Greece | [2]Institute of Quantum Materials and Technologies (IQMT), Karlsruhe Institute of Technology (KIT), Karlsruhe, Germany | [3]Facultad De Ciencias Naturales, Exactas y Tecnología, Depto. De Bioquímica, Universidad De Panamá, Panamá, Panama | [4]Facultad De Ciencias Naturales, Exactas y Tecnología, Grupo de Investigación de Materiales, Universidad De Panamá, Panamá, Panama | [5]Physikalisches Institut, Karlsruhe Institute of Technology (KIT), Karlsruhe, Germany | [6]Institute of Nanotechnology (INT), Karlsruhe Institute of Technology (KIT), Karlsruhe, Germany | [7]Facultad De Ciencias Naturales, Exactas y Tecnología, Depto. De Química-Física, Universidad De Panamá, Panamá, Panamá

Correspondence: Concepción Molina-Jirón (concepcion.moreno@kit.edu) | Eufemio Moreno-Pineda (eufemio.moreno@up.ac.pa) | Theocharis C. Stamatatos (thstama@upatras.gr)

Received: 31 January 2026 | **Revised:** 10 March 2026 | **Accepted:** 13 March 2026

ABSTRACT

A new dinuclear dysprosium(III) single-molecule magnet (SMM), $[Dy_2(hynad)_2(dbm)_4]\cdot DMF$ (**1**·DMF), supported by the bulky anionic N–O bridging ligand, N-hydroxy-1,8-naphthalimide ($hynad^-$), has been synthesized. The deprotonated $hynad^-$ ligands enforce a robust and nearly planar $\{Dy_2(\mu\text{-}OR)_2\}^{4+}$ core, which is surrounded by the sterically demanding dibenzoylmethanoate (dbm^-) coligands. Each Dy^{III} center adopts a distorted triangular dodecahedral geometry, generating a highly axial crystal field. AC magnetic measurements reveal zero-field SMM behavior, with slow relaxation of the magnetization persisting up to 16 K, as well as open magnetic hysteresis loops observed by μSQUID magnetometry up to 3.5 K. Analysis of the AC susceptibility data yields an effective energy barrier for magnetization reversal of $U_{eff} = 171$ K. μSQUID studies disclose a characteristic double-S-shaped hysteresis, consistent with an antiferromagnetically coupled ground state separated by a small energy gap from a low-lying ferromagnetic excited state. *Ab initio* calculations confirm the strongly axial $m_J = \pm 15/2$ ground Kramers doublets for both Dy^{III} ions, with the magnetic anisotropy axes oriented nearly perpendicular to the $\{Dy_2(\mu\text{-}OR)_2\}^{4+}$ plane. The combined experimental and theoretical analysis demonstrates that the Dy···Dy interaction is weak and predominantly dipolar in nature, with thermal population of the excited exchange-coupled state enabling the observed slow magnetic relaxation.

1 | Introduction

Single-molecule magnets (SMMs) are molecular systems that exhibit slow relaxation of magnetization arising from intrinsic molecular properties rather than long-range magnetic ordering [1]. Amongst the known SMMs, lanthanide-based systems play a central role in molecular magnetism due to their strong spin–orbit coupling and large magnetic anisotropy, with Dy^{III} being particularly effective for achieving high anisotropy [2–4]. Despite the effectiveness in achieving Dy-based SMMs, however, quantum tunneling of magnetization (QTM) often limits magnetic bistability in monometallic complexes [5, 6]. To mitigate this effect, dinuclear and multinuclear lanthanide architectures have been widely explored, as magnetic interactions between metal centers can suppress QTM and enhance magnetic relaxation barriers (U_{eff}) and blocking temperatures (T_B) [7].

In contrast to higher nuclearity clusters, Dy_2 systems provide well-defined and experimentally tractable models that enable disentanglement of the respective roles of single-ion anisotropy, dipolar and/or exchange interactions, governing magnetic relaxation [7, 8]. In such systems, the nature of the bridging ligand

---

(X) plays a decisive role, as it directly determines the Dy⋯Dy separation, the Dy–X–Dy connectivity, and the symmetry of the local coordination environment [9–13]. These factors collectively influence both the magnitude of magnetic coupling and the relative orientation of the local magnetic anisotropy axes, which are recognized as key parameters for suppressing efficient QTM and promoting slow magnetic relaxation. Consequently, rational control over the bridging motif in Dy_2 complexes has emerged as a powerful strategy for probing fundamental magneto-structural correlations and for optimizing single-molecule magnet behavior [8–13].

From a broader perspective, a wide variety of bridging ligands have been employed in the assembly of dinuclear Dy^{III} SMMs, among which oxygen-donor bridges involving a single bridging oxygen atom (μ-O) are the most prevalent. In particular, alkoxide (RO^-) [14–22], phenoxide ($R\text{-}PhO^-$) [23–32], and hydroxide (HO^-) [33–36] bridging ligands are among the most commonly encountered motifs, as they readily link two Dy^{III} ions and often enforce relatively short Dy⋯Dy separations, frequently resulting in a rhombus-shaped $\{Dy_2(\mu\text{-}O)_2\}^{4+}$ core. When combined with careful control over the coordination geometry and the imposition of strongly axial ligand fields at each Dy^{III} ion, several oxygen-bridged Dy_2 SMMs have been reported to exhibit large effective energy barriers (U_{eff}), in some cases reaching several hundred Kelvin [14–36]. Alternative strategies have focused on radical-bridged Dy_2 systems, in which inorganic (N_2^{3-}) or organic ligand radicals (e.g., tetrazine, tetrapyridylpyrazine, bipyrimidine, bis-benzimidazole, tetraazanaphthalene, fluoflavine) mediate magnetic exchange and introduce additional spin degrees of freedom [37–45]. These 2p-4f molecular systems can lead to enhanced exchange coupling between 4f-metal centers, mitigating the detrimental zero-field QTM relaxation process, thus yielding large coercive field values and higher magnetization blocking temperatures. Simpler halide bridging ligands (e.g., chloride, bromide, iodide) have also been explored, offering weakly donating, monoatomic connections that can preserve axial crystal fields and reduce perturbations to the Dy^{III} anisotropy, affording - in some cases- remarkably high effective barriers, in the range of 10^3 Kelvin [46–49]. It is worth mentioning that a recently reported triply iodide-bridged dinuclear organometallic Dy_2 complex represents a rare mixed-valence system, where μ_3-iodide ligation and direct Dy⋯Dy interactions give rise to exceptionally strong magnetic coupling and ultrahard single-molecule magnet behavior resulting in record coercive fields among all known SMMs to date [50].

Among the various bridging motifs explored in Dy_2 single-molecule magnets, N–O-based ligands have attracted considerable attention due to their ability to efficiently mediate magnetic exchange between highly anisotropic Dy^{III} centers. In particular, neutral pyridine N-oxides are now well established as effective μ-OR bridges, giving rise to a wide range of dinuclear Dy^{III} complexes with tunable magnetic behavior [51–71]. Significant progress in this area has demonstrated that simple pyridine-N-oxide bridges, when combined with β-diketonate ligands, can generate pseudo-axial DyO_8 coordination environments that efficiently suppress QTM and enable zero-field SMM behavior [53, 58, 60, 65, 66, 70]. This foundational structural motif has since been expanded through systematic modification of the N-oxide bridges, including substituted pyridine N-oxides, pyrazine-N-oxide, bipyridine N,N′-dioxides, and other heterocyclic or ditopic N-oxide ligands, most commonly in combination with hfac⁻ (hexafluoroacetylacetonate), tta⁻ (thenoyltrifluoroacetonate), or related ancillary β-diketonate ligands [51–71]. In contrast, anionic N–O-based ligands bearing a localized negative charge on the oxygen atom capable of supporting dinuclear Dy^{III} SMMs remain comparatively rare and underexplored [72, 73].

A notable contribution to this area was recently reported by some of us, by introducing the organic ligand *N*-hydroxy-1,8-naphthalimide (hynadH, Scheme 1A), which upon deprotonation can act as a new anionic N–O-based chelating and bridging ligand in dysprosium chemistry (Scheme 1B) [74]. In this reported work, a family of dinuclear complexes featuring a nearly planar $\{Dy_2(\mu\text{-}OR)_2\}^{4+}$ rhombus-shaped core was isolated (Scheme 1C),

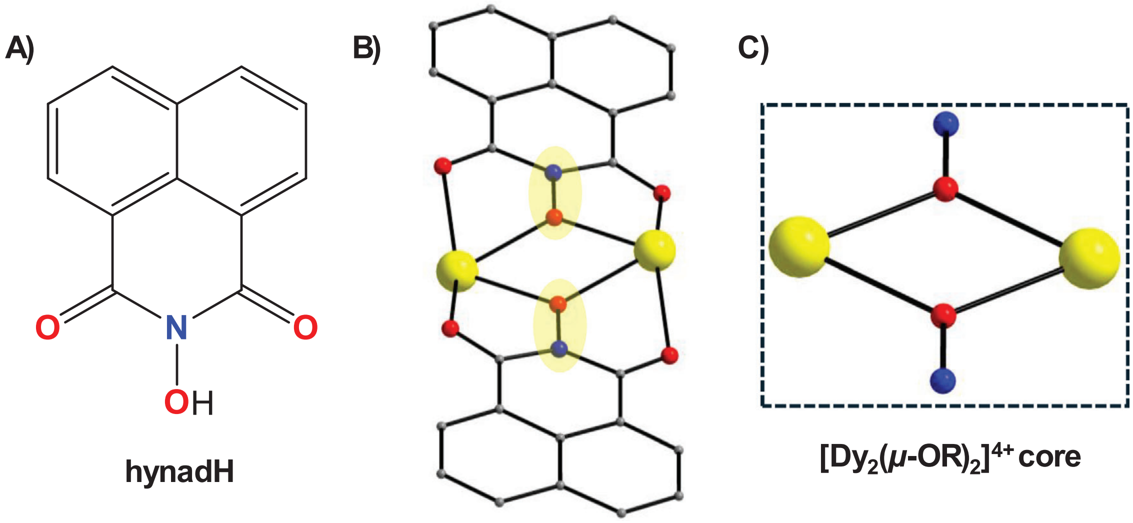

SCHEME 1 | (A) Chemical structure of the *N*-hydroxy-1,8-naphthalimide (hynadH) ligand, (B) bridging and chelating coordination mode of hynad⁻ forming the robust $[Dy_2(\mu\text{-}OR)_2]^{4+}$ core, and (C) rhombus-shaped $[Dy_2(\mu\text{-}OR)_2]^{4+}$ core resulting from the deprotonated N–O⁻ groups of hynad⁻. Color code: Dy^{III}, yellow; O, red; N, blue; C, dark gray.

demonstrating that the deprotonated $R_2N–O^-$ moiety can act as an efficient monoatomic bridge between two Dy^{III} centers while simultaneously chelating each metal ion. These studies firmly established hynad⁻ as a rare example of an anionic N–O-based ligand capable of stabilizing well-defined $\{Dy_2(\mu\text{-}OR)_2\}$ metal cores exhibiting SMM behavior [74]. Building upon this foundation, we further reported the structurally related dinuclear complex $[Dy_2(hynad)_2(dpm)_4]$, where dpm⁻ (dipivaloylmethanoate) ligands occupy the peripheral coordination sites while preserving the central $\{Dy_2(\mu\text{-}OR)_2\}^{4+}$ core enforced by the deprotonated *N*-hydroxy-1,8-naphthalimide bridges [75]. Notably, this compound exhibited pronounced SMM behavior, with a U_{eff} that was the highest reported to date among Dy_2 complexes constructed with the hynad⁻ bridging ligand. This result demonstrated not only the robustness of the $\{Dy_2(\mu\text{-}OR)_2\}^{4+}$ motif supported by hynad⁻, but also its capacity to promote favorable magnetic anisotropy and slow relaxation dynamics when combined with suitably chosen ancillary *β*-diketonate ligands.

In this context, the present study extends this chemistry through the synthesis and characterization of the closely related complex $[Dy_2(hynad)_2(dbm)_4]\cdot DMF$ (**1**·DMF), in which the peripheral dipivaloylmethanoate groups are replaced by the sterically demanding dibenzoylmethanoate ligands. Despite this substitution, the deprotonated *N*-hydroxy-1,8-naphthalimide ligands retain their *μ*-O bridging role, giving rise once again to a nearly planar $[Dy_2(\mu\text{-}OR)_2]^{4+}$ core. To gain a comprehensive understanding of the magnetic properties arising from this robust $[Dy_2(\mu\text{-}OR)_2]^{4+}$ core, we have undertaken a combined experimental and theoretical investigation of the aforementioned complex. In the present work, the magnetic behavior was examined using DC magnetometry to probe the static magnetic response and magnetic anisotropy, AC susceptibility measurements to characterize the slow relaxation of the magnetization and SMM behavior, and *μ*SQUID magnetometry to directly assess magnetic hysteresis down to the sub-Kelvin temperature regime. In parallel, *ab initio* calculations were performed to elucidate the electronic structure of the Dy^{III} centers, determine the orientation of the local magnetic anisotropy axes, and evaluate the nature and magnitude of the magnetic interactions transmitted through the $[Dy_2(\mu\text{-}OR)_2]^{4+}$ core. Hence, this combined approach allows a detailed structure-property correlation to be established and provides insight into the role of the $R_2N–O^-$ bridges in governing both the single-ion anisotropy and the intramolecular Dy⋯Dy magnetic coupling.

2 | Results and Discussion

2.1 | Synthetic Comments

Following our previous works on dinuclear dysprosium complexes supported by the anionic N–O-based ligand hynad-, in which systematic modulation of peripheral coordination environments was achieved through variation of nitrate and *β*-diketonate ligands, we sought to further expand this family by introducing sterically more demanding *β*-diketonates. In analogy with the reported syntheses of $[Dy_2(hynad)_2(dpm)_4]$ and related systems [74, 75], the reaction between $Dy(dbm)_3\cdot H_2O$ and hynadH in the presence of Et_3N was carried out using a 1:1:1 molar ratio in a CH_2Cl_2/DMF solvent mixture (5:1, v/v). Under these mild basic conditions, deprotonation of hynadH promotes formation of the characteristic double N–O-bridged $\{Dy_2(\mu\text{-}OR)_2\}^{4+}$ core, while the bulky dibenzoylmethanato ligands occupy the remaining coordination sites and impose increased steric pressure on the dinuclear unit. This approach afforded well-shaped block-like yellow crystals of the dinuclear complex $[Dy_2(hynad)_2(dbm)_4]\cdot DMF$ (**1**·DMF), suitable for single-crystal X-ray diffraction. Notably, despite replacement of the less bulky dpm⁻ chelates [74, 75] with dbm⁻, the robust and nearly planar $\{Dy_2(hynad)_2\}^{4+}$ core is retained, highlighting the structural directing role of the hynad⁻ ligand and its ability to stabilize dinuclear metallic assemblies across a range of different ancillary ligand environments.

2.2 | Description of Structure

Crystallographic details and selected interatomic distances and angles for compound **1**·DMF are listed in Tables S1 and S2, respectively. For the sake of brevity, only the important metrical parameters will be discussed in the main text. Single-crystal X-ray diffraction analysis reveals that compound **1**·DMF is a dinuclear Dy^{III} complex with the molecular formula $[Dy_2(hynad)_2(dbm)_4]$ (Figure 1A). Complex **1**·DMF crystallizes in the trigonal space group *R*3*c*, and its crystal packing is stabilized by one lattice DMF molecule per dinuclear unit. The asymmetric unit consists of a dinuclear Dy^{III} complex containing two crystallographically unique metal centers (Dy1 and Dy2). These metal centers are doubly bridged by the $R_2N–O^-$ groups (through O10 and O13 atoms) of two deprotonated hynad⁻ ligands, yielding a rhombus-shaped $\{Dy_2(\mu\text{-}OR)_2\}^{4+}$ core. The $\{Dy_2(\mu\text{-}OR)_2\}^{4+}$ core, which consists of two tridentate chelating and bridging ($\eta^1{:}\eta^2{:}\eta^1{:}\mu$) hynad⁻ ligands arranged opposite to each other, is further stabilized by the formation of two five-membered chelate rings from each hynad⁻ ligand, involving the two carbonyl oxygen atoms (O9, O11 and O12, O14) and the oxygen atoms (O10 and O13) of the $R_2N–O^-$ groups. Peripheral coordination in complex **1**·DMF arises from four O,O′-chelating dbm⁻ ligands (O1, O2, O3, O4 for Dy1 and O5, O6, O7, O8 for Dy2) located above and below the plane of the central metal core, resulting in a DyO_8 coordination environment for each metal ion. Both Dy^{III} ions are thus 8-coordinate, and according to the SHAPE program, they adopt distorted triangular dodecahedral coordination geometries (Figure 1B) with similar CShM values (3.38 for Dy1 and 3.22 for Dy2, Table S3). The similarity in the coordination polyhedra is further confirmed by the almost identical Dy–O bond distances and O–Dy–O bond angles between Dy1 and Dy2 units. The intradimer Dy1⋯Dy2 distance is 3.993(8) Å while the Dy1–O10–Dy2 and Dy1–O13–Dy2 angles are 118.5(1)° and 118.1(1)°, respectively. Likewise, the shortest intermolecular Dy⋯Dy distance resulting from two adjacent dimeric Dy_2 complexes is 9.067(5) Å. Interestingly, the Dy_2 complexes (Figure S1a) are densely packed and interconnected through extensive *π*–*π* stacking interactions between the naphthalene backbone of the hynad⁻ ligands and the twisted phenyl rings of the dbm⁻ ligands of neighboring Dy_2 units. The corresponding centroid-to-centroid distances are 3.643 and 3.662 Å (Figure S2). Viewed along the crystallographic *c*-axis, the dinuclear Dy_2 units adopt a cyclic supramolecular arrangement in which the phenyl rings of the peripheral dbm⁻ ligands are oriented toward the interior of the assembly, giving rise to star-like packing motifs stabilized by *π*–*π* interactions (Figure S1b).

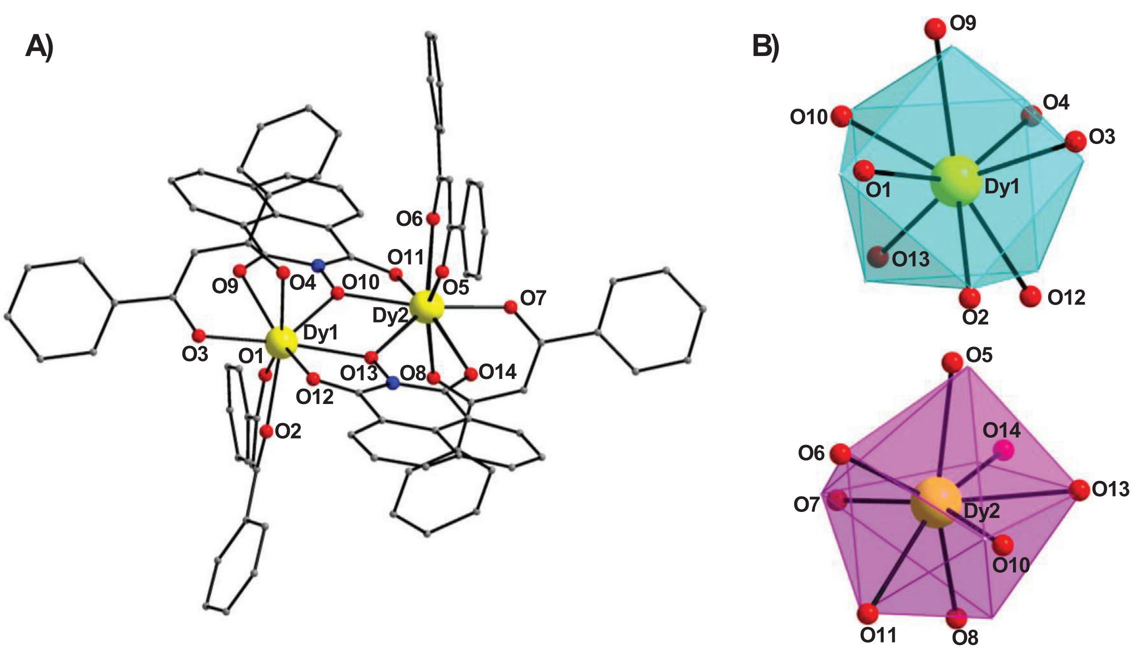

FIGURE 1 | (A) Labeled representation of the crystal structure of complex **1**·DMF, and (B) triangular dodecahedral coordination polyhedra of the crystallographically independent Dy^{III} metal centers in complex **1**·DMF. The smaller white spheres define the vertices of the corresponding ideal polyhedron. All H atoms and the DMF lattice solvent are omitted for clarity. Color code: Dy^{III}, yellow; O, red; N, blue; C, dark gray.

2.3 | Magnetic Studies

2.3.1 | Static Magnetic Properties

Direct-current (DC) magnetic susceptibility measurements were performed on a microcrystalline sample of **1** over the temperature range 1.9–300 K under an applied magnetic field of 0.1 T (Figure 2A). The chemical purity of the sample used for the magnetic studies was confirmed by elemental analysis, allowing accurate determination of its exact molecular weight. The room temperature $\chi_M T$ value of 27.8 $cm^3\ mol^{-1}$ K is very close to the theoretical value of 28.3 $cm^3\ mol^{-1}$ K for two noninteracting Dy^{III} ions ($^6H_{15/2}$, $S = 5/2$, $L = 5$ and $g = 4/\,3$). Upon cooling, the $\chi_M T$ value decreases gradually down to 8 K, and it then drops abruptly before reaching a value of 14.8 $cm^3\ mol^{-1}$ K at the lowest measured temperature (2 K). The rapid decline of $\chi_M T$ at low temperatures is attributed to the depopulation of the m_J sublevels of the ground J state, and possibly to the presence of weak antiferromagnetic interactions between the two Dy^{III} ions.

The field (H) dependence of the magnetization (M) for complex **1** measured at 2, 3, 4, and 5 K is shown in Figure 2B. The magnetization increases rapidly at low applied fields but does not reach full saturation even at the maximum applied field of 7 T, indicating the presence of significant magnetic anisotropy and/or low-lying excited states. At 2 K, the magnetization tends toward saturation above approximately 2 T, reaching a value of 10.4 $N\mu_B$ at 7 T. This value is significantly lower than the expected saturation magnetization (M_{sat}) value for two noninteracting Dy^{III} ions ($M_{sat}/N\mu_B = 20\ N\mu_B$), reflecting strong magnetic anisotropy and crystal-field effects.

2.3.2 | Dynamic Magnetic Properties

To investigate the magnetization relaxation dynamics of complex **1** and to validate its SMM properties, alternating current (AC) magnetic susceptibility measurements were initially performed at zero applied DC field in the temperature range of 1.8–18 K, under an AC field of 3.0 Oe, with frequencies ranging from 0.1 to 1512 Hz. The pronounced frequency- and temperature-dependent behavior of both the in-phase ($\chi_M{}'$) and out-of-phase ($\chi_M{}''$) magnetic susceptibilities unambiguously confirms SMM behavior in the absence of an applied DC field for complex **1** (Figures 3 and S3–S5). Interestingly, the temperature dependence of the out-of-phase AC magnetic susceptibility, $\chi_M{}''(T)$, exhibits a well-resolved maximum at 16 K at the highest frequency of 1512 Hz (Figure S5A). Frequency-dependent magnetic susceptibility ($\chi_M{}''(\nu)$) studies revealed a maximum centered at 0.2 Hz at the lowest temperature of 2 K. This maximum remains essentially temperature independent upon increasing the temperature up to 4 K, due to the dominant QTM relaxation. Above 4 K, the peak maxima become distinctly temperature dependent, progressively shifting toward higher frequencies with increasing temperature, due to the onset of phonon-assisted relaxation pathways (Raman and Orbach mechanisms). In addition, the shapes of the Cole-Cole plots deviate from the typical semicircular ones, yielding α values in the range of 0.40–0.05 (Table S4), indicative of a wide distribution of relaxation times, which is consistent with the presence of multiple relaxation processes. Furthermore, the $\chi_M{}'T$ value ($\chi_M{}'$ being the in-phase AC susceptibility) at its plateau temperature region is ~25 cm^3 K mol^{-1} (Figure S3B), which is very close to the expected value (~27 cm^3 K mol^{-1}) for randomly oriented crystals of a molecule with two strongly anisotropic Dy^{III} ions, each with a $m_J = \pm 15/2$ Ising ground Kramers' doublet [76].

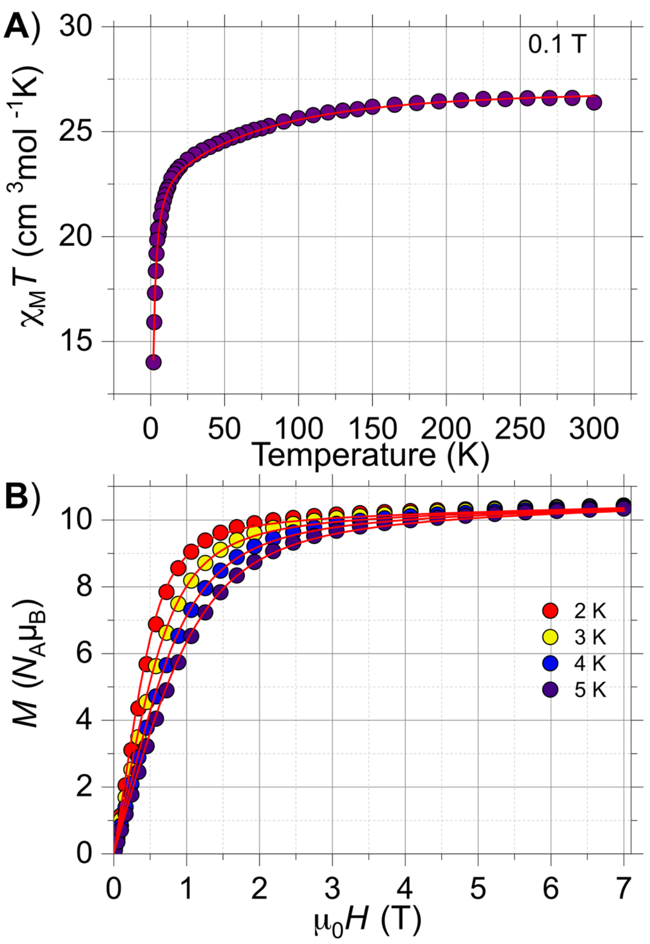

FIGURE 2 | Temperature dependence of the $\chi_M T$ product at 0.1 T static DC field (A) and field (H) dependence of the magnetization (M) at four different low temperatures (B) for complex **1**. Experimental data are shown as filled circles. Solid lines are $\chi_M T(T)$ and $M(H)$ traces obtained employing the crystal field parameters from CASSCF calculations (see the text for details).

The relaxation times (τ) can be extracted from the AC magnetic susceptibility data by simultaneously fitting $\chi_M'(\nu)$ and $\chi_M''(\nu)$ in the range of 2–18 K employing a generalised Debye model. The temperature dependence of the relaxation times at zero DC field can be fitted employing the QTM, Raman and Orbach processes by using the following Equation (1) [77, 78]:

$$\tau^{-1} = \tau_0^{-1} \exp\left(-U_{\text{eff}}/k_B T\right) + CT^n + \tau_{QTM}^{-1} \tag{1}$$

where τ^{-1} defines the relaxation rate, and the first term corresponds to the Orbach process in which τ_0 is the pre-exponential factor, $k_\text{B}T$ is the thermal energy, and U_eff is the effective energy barrier for the magnetization reversal. In addition, C and n are parameters of the Raman relaxation, and $\tau_\text{QTM}{}^{-1}$ is the rate of the QTM process. The best-fit of the data (solid red line in Figure 4A) yielded the values: $\tau_0 = 6.8(3) \times 10^{-9}$ s, $U_\text{eff} = 119(1)$ cm^{-1} [171(1) K], $C = 1.36(4) \times 10^{-2}$ s^{-1} K^{-n}, $n = 4.52(3)$, and $\tau_\text{QTM} = 0.65(2)$ s. The U_eff value of complex **1** is of similar magnitude with those reported for the highest performing pyridine N-oxide bridged Dy$_2$ SMMs supported by β-diketonate ligands (Table S5).

To reduce the contribution of QTM on the magnetization relaxation, AC magnetic susceptibility measurements were performed under an applied optimal DC field of 750 Oe (see Figures S6 and S7). As a result, the low-temperature tails observed in the $\chi_M''(T)$ plots were strongly suppressed and ultimately vanished (Figure S5), indicating efficient quenching of QTM. The removal of these features has contributed toward the slowing of the relaxation process and the shifting of the χ_M'' peak maxima outside the experimental frequency window (Figure 3C). Under the applied DC field of 750 Oe, the $\chi_M''(\nu)$ maxima measured at different temperatures have become more clearly resolved, leading to improved separation of the peaks compared to the zero-field AC data (Figures 3A and 3C). The shape of the Cole-Cole plots in the presence of a DC field is more circular and less asymmetric than in zero field, especially at low temperatures, yet denoting a wide distribution of relaxation times, as evidenced by the α values in Table S6. In this case, the temperature dependence of relaxation times was modelled by excluding the QTM term (solid red line in Figure 4B), using the following Equation (2):

$$\tau^{-1} = \tau_0^{-1} \exp\left(-U_{\text{eff}}/k_B T\right) + CT^n \tag{2}$$

The relaxation parameters obtained under an applied DC field of 750 Oe are: $\tau_0 = 1.1(1) \times 10^{-8}$ s, $U_\text{eff} = 117(4)$ cm^{-1} [169(6) K], $C = 3.8(4) \times 10^{-2}$ s^{-1} K^{-n}, $n = 5.0(2)$. Although the application of an external DC field reduces QTM at the lowest temperatures, it does not lead to any increase in the energy barrier for magnetization reversal. The obtained Raman parameters, C and n, are within the expected range for Dy$^\text{III}$-based SMMs [14–50]. The observed lower n values ($n = 9$ for Kramers ions) are possibly attributed to the presence of low-energy phonon modes and/or slight deviations from ideal Raman relaxation [79–81]. Intriguingly, the $\tau(H)$ study (Figure S7), besides providing the field at which relaxation is slowest, also shows fast relaxation occurring at 0.18 T.

2.4 | µSQUID Hysteresis Studies

Confirmation of the SMM characteristics of complex **1** was obtained by investigating its magnetic hysteresis behavior. For this, a sub-kelvin investigation was carried out employing highly sensitive µSQUID arrays. The µSQUID measurements were performed on single crystals of complex **1**·DMF with the field applied along the easy axis of the crystal, employing the transverse field method [82]. The studies comprise field sweep rates from 64 mT/s down to 1 mT/s and temperatures ranging from 30 mK up to 5 K.

µSQUID measurements revealed open hysteresis loops for the Dy$_2$ complex at the lowest measured temperatures (30 mK) that remain open until 3.5 K (Figure 5B), while the sweep-rate-dependent loops highlight the expected behavior of SMMs (Figure 5A). Moreover, at the lowest temperature, the dimeric nature of the complex is readily visible, as shown by the double-S-shaped hysteresis loops, typical of an antiferromagnetically coupled Dy$_2$ SMM [26, 30, 83–86]. At high negative field and 30 mK temperature, the ferromagnetically coupled excited state is populated. Upon decreasing the field, a crossing with the antiferromagnetically coupled ground state occurs at -0.18 T. Between the ±0.18 field, nearly no magnetic moment is observed,

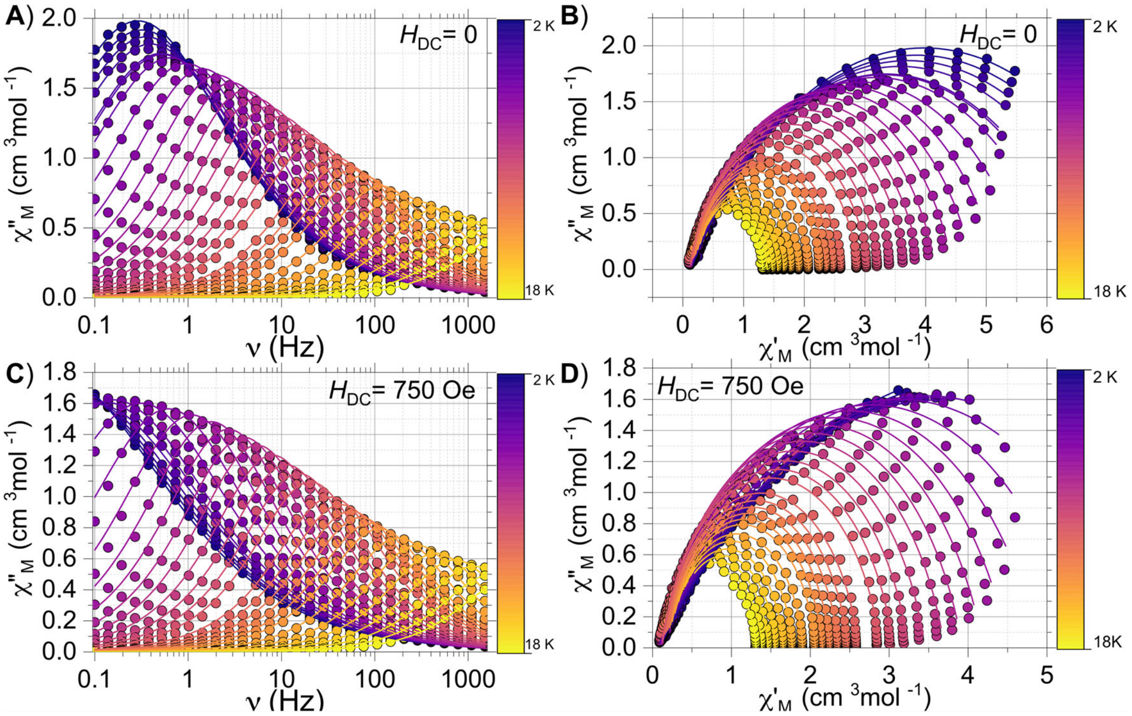

FIGURE 3 | Frequency-dependence of the out-of-phase (χ_M'') AC magnetic susceptibility over the temperature range 2-18 K, at zero DC field (A), and under an applied field of 750 Oe (C) for complex **1**. Cole-Cole plots for complex **1** obtained using the AC susceptibility data at zero DC field (B), and under an applied field of 750 Oe (D). Solid lines represent the best fit to a generalized Debye model.

as expected for a purely diamagnetic ground state. Above +0.18 T, a crossing between the antiferromagnetic ground state and the excited ferromagnetic state occurs, leading to the progressive population of the ferromagnetic ground state (Figure 5A). The fast relaxation observed in the $\tau(H)$ dependence from the AC susceptibility measurements can therefore be attributed to enhanced QTM at the level crossing between the exchange-coupled ground and first excited states (Figure S7).

Additionally, within ±0.18 mT, the magnetic moment is nearly zero at the lowest temperatures due to the diamagnetic ground state; upon increasing temperature, thermal population of the ferromagnetic excited state leads to a progressive increase in the magnetization in this field region, as evidenced by the comparison between the 30 mK hysteresis loops and those recorded at higher temperatures (Figure 5B). The inflection points observed in the μSQUID loops allow the determination of the mean exchange field (H_{ex}), leading to an effective exchange constant between the Ising spins of the Dy$^{\text{III}}$ ions according to the following Equation (3):

$$H_{ex} = \frac{-2\,J_{ex} m_J}{g_J \mu_B} \tag{3}$$

where m_J = 15/2 and g_J = 4/3 [30, 87]. This leads to an effective exchange constant of J_{ex} = -0.0066 cm^{-1} (-9.5 mK). The determined J_{ex} of -9.5 mK is close to the value obtained from a purely point dipolar approximation: D_{dip} = -5 mK for a Dy⋯Dy distance of 3.993(8) Å, suggesting that the interaction between the Dy$^{\text{III}}$ atoms is most likely purely of dipolar origin, although exchange cannot completely be excluded [30].

2.5 | Theoretical Calculations

To comprehend the magnetic characteristics of complex **1**, we carried out *ab initio* calculations using the CASSCF/SO-RASSI/SINGLE_ANISO approach (see the *ab initio* section for details). For this purpose, the crystal structure of the Dy$_2$ complex was employed without further optimization. The energies of the low-lying Kramers doublets (KDs), the main components of the *g*-tensor, along with the m_J components for each KD for Dy1 and Dy2, are shown in Tables S7 and S8, respectively. Inspection of the low-lying electronic structure of both Dy$^{\text{III}}$ ions revealed highly axial *g*-values in the ground $\pm m_J$ states approaching the Ising limit, i.e., $g_x = g_y \sim 0$ and $g_z \sim 20$. The ground KDs for both Dy$^{\text{III}}$ ions at the Dy$_2$ complex are predominantly comprised of a $m_J = \pm 15/2$ doublet (> 98%), while the first excited states are found to be highly mixed. For Dy1, the first excited state is found to lie at 118 cm^{-1}, while for Dy2, the excited state lies at 84 cm^{-1}. The easy axes of magnetization lie nearly perpendicular to the plane defined by both Dy$^{\text{III}}$ ions and the R$_2$N–O$^-$ groups from the hynad$^-$ ligands, corresponding to the central $\{\text{Dy}_2(\mu\text{-OR})_2\}^{4+}$ core, as depicted in Figure 6. Specifically, the magnetic anisotropy vectors of Dy1 and Dy2 are aligned along the axial O4 and O8 atoms of the dbm$^-$ ligands, respectively. This alignment arises from the relatively short Dy–O bond distances, which dominate the local crystal field environment [88].

Although the CASSCF results indicate that the single-ion characteristics for each Dy$^{\text{III}}$ resulting from the crystal field environment are highly anisotropic, with a relatively large energy separation between the ground and first excited $\pm m_J$ states, the magnetic behavior must also take into account the presence of interactions

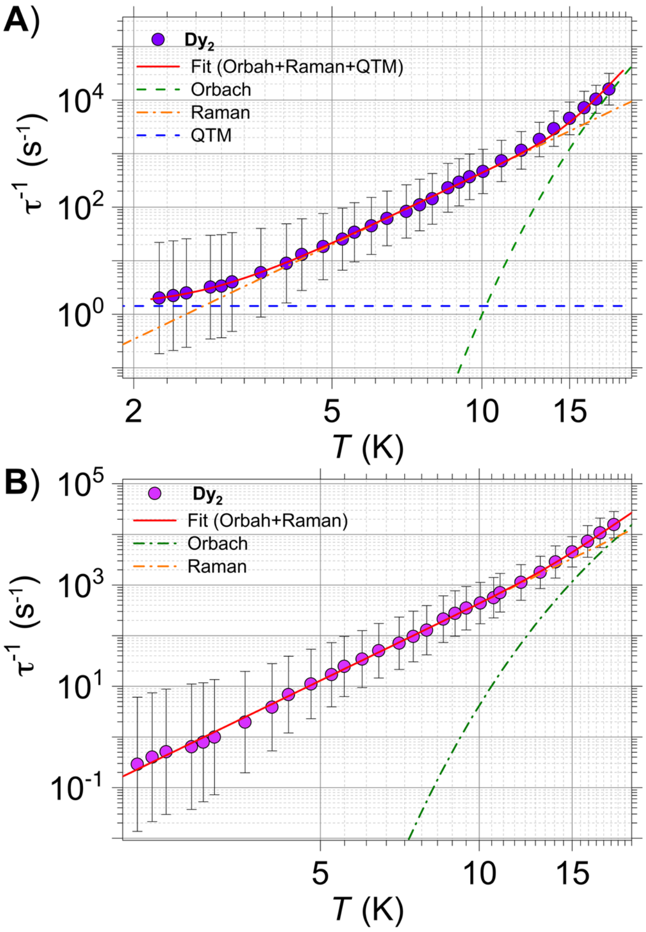

FIGURE 4 | Temperature dependence of the relaxation rates (τ^{-1}) at zero DC field (A), and under an applied DC field of 750 Oe (B), fitted by implementing Equations (1) and (2), respectively. The solid circles correspond to the experimental data, while the continuous red solid line represents the best fit obtained from the above equations. The individual contribution of each relaxation process is illustrated as dashed lines, and error bars represent the standard deviations in the relaxation rates obtained from the fitting of the AC susceptibility data.

operating between the Dy$^{\text{III}}$ atoms. With the knowledge of the crystal field parameters from CASSCF (Table S9), it is possible to evaluate whether the downturn in the $\chi_M T(T)$ data corresponds to the two interacting Dy$^{\text{III}}$ ions. For this, we employed the Lines model by simultaneously fitting the $\chi_M T(T)$ and $M(H)$ data sets [89]. The Lines model employs an isotropic exchange between the spin component of the angular momenta ($S = 5/2$ for Dy$^{\text{III}}$) and the crystal field parameters obtained from the CASSCF calculations. The Hamiltonian is described by the following Equation (4):

$$\mathcal{H}^i_{Dy} = \mathcal{H}^i_{lf} + g_J \mu_0 \mu_B \left(\hat{J}_{Dy1} + \hat{J}_{Dy2}\right) H_z - 2J^i_{\text{Lines}} \left(\hat{S}_{Dy1} \cdot \hat{S}_{Dy2}\right) \quad (4)$$

where $\mathcal{H}^i_{lf} = \sum_{k=2,4,6,-k\leq q\leq k} B^q_k O^q_k$ is the ligand field Hamiltonian expressed in the Steven's operators, O^q_k are the Stevens operators, and B^q_k are the ligand field parameters obtained from CASSCF calculations. In addition, $\hat{J}_{Dy}$ and $\hat{S}_{Dy}$ are the spin-orbit and spin-only states for each Dy$^{\text{III}}$ atom, respectively. Simultaneous fit of the $\chi_M T(T)$ and $M(H)$ data has yielded a J_{Lines} = -0.0046(1) cm^{-1} (6.6 mK) (see solid lines in Figure 2) [90]. Considering the interaction operating within the dimer, the ground doublet state is a singlet, with a separation of ~1 cm^{-1} from the first excited state multiplet. Considering that the separation is small and the operating temperature of our experiments (> 2K), the excited state is readily populated, hence the SMM character in this system arises from the first excited multiplet state. Above this state, the next excited multiplet lies at ~86 cm^{-1}, which coincidentally is very close to the U_{eff} determined from the AC studies, thus relaxation occurs via this state.

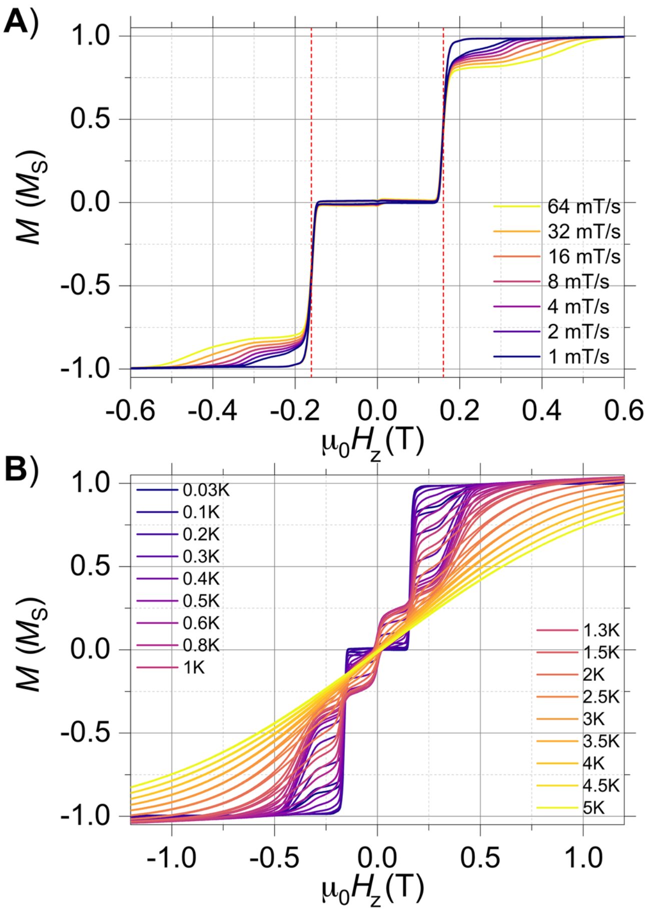

FIGURE 5 | µSQUID hysteresis loops: (A) Sweep-rate dependence of the $M(H)$ data for Dy$_2$ recorded at 30 mK. The inflection points at ±0.18 T (red dotted lines), and the nearly flat region indicate an antiferromagnetic ground state and the presence of a mean exchange field operating between the Dy$^{\text{III}}$ ions. (B) Temperature dependence of the $M(H)$ loops measured between 30 mK and 3.5 K at a field sweep rate of 16 mT/s, leading to open hysteresis loops and demonstrating the slow magnetic relaxation characteristics of complex **1**·DMF.

Although a direct comparison of the J_{Lines} and the J_{ex} is not possible, projecting the J_{Lines} for a $S = 5/2$ into a $J = 15/2$ state leads to a value of J_{Lines} (15/2) = -0.005 cm^{-1} (-7 mK), close to the experimentally obtained J_{ex} of -9.5 mK. This is readily visible when comparing the derivative of the temperature dependence of the $M(H)$ loops and the Zeeman diagram employing the Lines model (Figure 7). As shown in Figure 7, the extremely narrow remanence is indicative of an antiferromagnetic ground state persisting within ±0.18 T, as confirmed by the first-derivative magnetization curves (dM/dH). In this field region, the

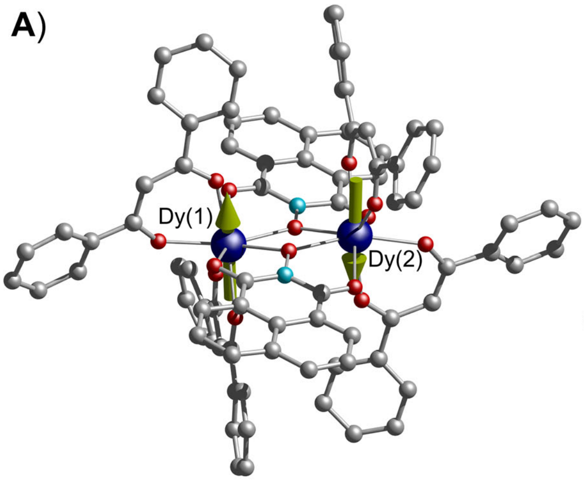

FIGURE 6 | Side (A) and top (B) views of the calculated orientations of the principal axes (green arrows) of the g-tensors for the ground Kramers doublets of Dy1 and Dy2 in complex **1**. Color code: Dy, blue; C, gray; N, cyan; O, red. Hydrogens were omitted for clarity.

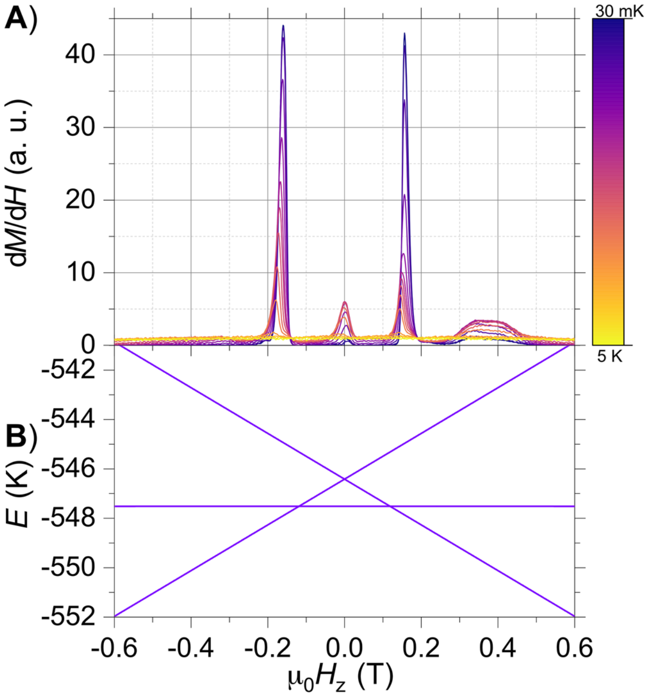

FIGURE 7 | (A) Derivative of the temperature-dependent $M(H)$ hysteresis loops at 16 mT/s and (B) Zeeman diagram obtained employing the crystal field parameters from CASSCF and the J_{Lines} obtained from fitting the $\chi_M T(T)$ and $M(H)$ data.

magnetization is essentially zero. The sharp peaks observed in the dM/dH plot at ±0.18 T are nearly coincident with the predicted Zeeman crossings (red dotted lines in Figure 7) between the antiferromagnetic ground state (horizontal line) and the first excited ferromagnetic state. Beyond these field limits, the thermal population of magnetic states gives rise to SMM behavior, with switching fields that closely match the computationally determined intramolecular magnetic field (0.12 T) from the Zeeman diagram. The small peak observed at zero field in the dM/dH plot exhibits a strong temperature-dependent behavior and is attributed to a level crossing within the ferromagnetic state, which enables QTM once this excited state becomes thermally populated. Note that a broad peak centered at ~0.35 T can be ascribed to magnetization relaxation via a direct process [30].

Knowledge of the low-lying electronic structure of the dimeric Dy$^{\mathrm{III}}$ complex enables a rational interpretation of its static and dynamic magnetic behavior. The single-ion anisotropy, along with the local crystal field environment of the Dy$^{\mathrm{III}}$ ions, is responsible for the SMM behavior in complex **1** [2, 91]. However, at the single-ion level, the magnetic characteristics of these systems would be dominated by QTM at zero field, as is often observed in hysteresis studies with a sharp drop of magnetization (butterfly-shaped loops) [5, 6, 26]. In contrast, the antiferromagnetic interaction between the Dy$^{\mathrm{III}}$ pairs causes the zero-field QTM process to shift away from zero field to higher fields, as evidenced by the S-shaped μSQUID loops. Although the ground-coupled state is nonmagnetic due to the antiferromagnetic interaction– hence, no SMM properties would be expected– the small separation (~1 cm^{-1}) between the ground (nonmagnetic) and the first excited (ferromagnetic) exchange doublet leads to a considerable population of the latter even at 2 K, causing the response observed in the AC data.

2.6 | Conclusions

In summary, we have synthesized and comprehensively characterized a new dinuclear Dy$^{\mathrm{III}}$-based single-molecule magnet with formula [Dy$_2$(hynad)$_2$(dbm)$_4$] (**1**), supported by a bulky anionic N–O-based bridging ligand. The coordination complex features a robust and nearly planar $\{\mathrm{Dy_2}(\mu\text{-OR})_2\}^{4+}$ core enforced by two deprotonated *N*-hydroxy-1,8-naphthalimide (hynad$^-$) ligands, demonstrating that this anionic N–O bridging motif reliably stabilizes dimeric Dy$^{\mathrm{III}}_2$ complexes in the presence of sterically demanding *β*-diketonate coligands.

Magnetic studies establish zero-field SMM behavior, with slow magnetic relaxation until 16 K, as evidenced by AC susceptibility measurements, and open hysteresis loops persisting up to 3.5 K.

Analysis of temperature-dependent relaxation times yields an effective energy barrier of $U_{\text{eff}} = 119\ \text{cm}^{-1}$ (~171 K). µSQUID measurements reveal a characteristic double-S-shaped hysteresis, consistent with an antiferromagnetically coupled ground state and a low-lying ferromagnetic excited state responsible for the observed SMM behavior. *Ab initio* calculations confirm the highly axial nature of the two Dy^{III} ions, with ground KDs dominated by $m_J = \pm 15/2$ character and the principal magnetic anisotropy axes oriented nearly perpendicular to the $\{\text{Dy}_2(\mu\text{-OR})_2\}^{4+}$ plane. The combined experimental and theoretical analysis shows that the intramolecular Dy···Dy interaction is weak and predominantly dipolar in origin, giving rise to an antiferromagnetic ground state separated by a small energy gap (~1 cm^{-1}) from the first excited ferromagnetic exchange doublet. Thermal population of this excited state enables slow magnetic relaxation, with the Orbach process proceeding via higher-lying exchange-coupled states (~86 cm^{-1}) that are consistent with the experimentally determined relaxation barrier.

Overall, this work highlights the effectiveness of anionic N–O-based bridging ligands as versatile and underexplored building blocks for dinuclear lanthanide single-molecule magnets. The hynad^- ligand, in particular, provides a powerful structural platform that enables systematic tuning of peripheral coordination environments while maintaining favorable magnetic anisotropy and exchange characteristics. These findings expand the family of high-performance and air-stable Dy_2 SMMs, paving the way for further development of N–O-bridged molecular nanomagnets with enhanced magnetic bistability.

2.7 | Experimental

2.7.1 | Synthesis

All manipulations were performed under aerobic conditions using materials (reagent grade) and solvents as received unless otherwise noted. The $\text{Dy(dbm)}_3\cdot\text{H}_2\text{O}$ starting material was synthesized following a similar reported procedure [75]. The identity and purity of the solid-state product were confirmed by Fourier-transform infrared (FT-IR) spectroscopy and elemental analysis.

$[\text{Dy}_2(\text{hynad})_2(\text{dbm})_4]\cdot\text{DMF}$ (**1**·DMF). To a stirred, orange colored solution of hynadH (0.10 mmol, 0.021 g) and Et_3N (0.10 mmol, 0.014 mL) in a solvent mixture of CH_2Cl_2 and DMF (12 mL, 5:1, v/v), was added $\text{Dy(dbm)}_3\cdot\text{H}_2\text{O}$ (0.10 mmol, 0.079 g), resulting in a yellow-colored solution. The solution was stirred for 15 min, then filtered, and the filtrate was left to evaporate slowly at room temperature. After 3 - 4 days, X-ray quality dark yellow block-like crystals of **1**·DMF appeared. These were collected by filtration, washed with cold CH_2Cl_2 (2 × 2 mL) and Et_2O (2 × 5 mL), and dried in air. Yield: 43 %. Anal. calc. (found) for $\text{C}_{87}\text{H}_{63}\text{Dy}_2\text{N}_3\text{O}_{15}$ (**1**·DMF): C 60.91 (60.98), H 3.70 (3.79), N 2.45 (2.41). Selected FT-IR data (cm^{-1}): 3059 (w), 3026 (w), 1668 (s), 1644 (m), 1596 (s), 1550 (s), 1516 (s), 1477 (m), 1454 (s), 1388 (vs), 1284 (s), 1253 (m), 1221 (s), 1177 (w), 1157 (w), 1125 (w), 1071 (m), 1045 (s), 1023 (23), 997 (w), 908 (vs), 844 (s), 811 (w), 778 (s), 756 (m), 720 (s), 685 (s), 609 (m), 548 (w), 518 (s), 452 (w), 430 (w).

2.7.2 | Single Crystal X-Ray Crystallography

Data for compound **1**·DMF were collected on a Rigaku XtaLAB Synergy-S single-crystal X-ray diffractometer equipped with a CCD area detector and a graphite monochromator utilizing Cu Kα radiation (λ = 1.54184 Å). A selected block-like yellow crystal of **1**·DMF (0.232 × 0.186 × 0.128 mm) was attached to a glass fiber with paratone-N oil and transferred to a goniostat for data collection. Empirical absorption corrections (multiscan based on symmetry-related measurements) were applied using CrysAlis RED software [92]. The structures were solved by direct methods using SIR92 [93], and refined on F^2 using SHELXL97 [94], SHELXL-2014/7 [95], and SHELXT [96]. Software packages used: CrysAlisCCD [92] for data collection, CrysAlisRED [92] for cell refinement and data reduction, and WINGX for geometric calculations [97]. All the non-H-atoms were treated anisotropically, whereas the H-atoms were placed at calculated, ideal positions and refined as riding on their respective C-atoms. Various figures of all the structures were created using Mercury [98] and Diamond [99] software packages.

2.7.3 | Physical Measurements

Elemental analyses (C, H, and N) were performed by the University of Patras microanalytical service. Infrared (IR) spectra (4000–400 cm^{-1}) were recorded in the solid state using a Perkin–Elmer16 PC spectrometer with samples prepared as KBr pellets. Magnetic susceptibility measurements were conducted in a Quantum Design MPMS-XL SQUID magnetometer on a polycrystalline sample of complex **1** in the temperature range of 2–300 K with an applied DC magnetic field of 1 kOe. The DC data were corrected for diamagnetic contributions from the sample holder and eicosane. Core diamagnetic corrections were performed employing Pascal's constants [100]. The AC data was collected in an oscillating magnetic field of 3.5 Oe and frequencies between 1 and 1.5 kHz. Low temperature (0.03–5 K) magnetization (M) versus field (H) studies were performed on single crystals of complex **1**·DMF employing a µSQUID array inside a dilution refrigerator equipped with a 3D vector magnet [101]. The high sensitivity of this magnetometer allows the study of single crystals of SMMs of the order 10–500 µm. The time resolution was approximately 1 ms. The magnetic field was applied in different directions of the µSQUID plane with a precision better than 0.1° by driving three orthogonal coils separately. To ensure good thermalization, each sample was fixed with Apiezon grease.

2.7.4 | *Ab Initio* Calculations

Ab initio calculations were performed on complex **1** using the CASSCF/SO-RASSI/SINGLE_ANISO approach implemented in the OpenMolcas package [102–105]. For the calculations, the crystal structure was employed without further optimizations, and the atoms were described using the standard basis sets from the ANO-RCC library [106–108]. Due to the presence of two distinct Dy^{III} ions in the molecule, the dilution method was employed, where the Dy^{III} ion of interest was swapped with Y^{III} for the computations. Two calculations were conducted.

A basis set of VTZP quality was employed for the Dy^{III} ions, while VDZP quality was employed for atoms directly bound to the Dy^{III} ions, and VDZ quality for the remaining atoms, using the second-order DKH transformation [109]. Optimization of the molecular orbitals (MOs) was achieved by state-averaged CASSCF calculations. The active space of Dy^{III} was defined by the nine 4f electrons in the seven 4f orbitals. Three calculations were carried out (RASSCF routine) with 21, 224, and 490 states for $S = 5/2$, $S = 3/2$, and $S = 1/2$, respectively. The CASSCF wavefunctions were subsequently mixed by spin-orbit coupling, employing the RASSI routine [110–112] with all 21 states for $S = 5/2$ being included, while 128 and 130 states were included for $S = 3/2$ and $S = 1/2$. Lastly, the crystal field decomposition of the ground $J = 15/2$ multiplet of the $^6H_{15/2}$ term was executed with the SINGLE_ANISO module.

Acknowledgment

The publication of this article in OA mode was financially supported by HEAL-Link.

Conflicts of Interest

The authors declare no conflicts of interest.

References

1. A. Zabala-Lekuona, J. M. Seco, and E. Colacio, “Single-Molecule Magnets: From Mn12-ac to Dysprosium Metallocenes, a Travel in Time,” *Coordination Chemistry Reviews* 441 (2021): 213984, https://doi.org/10.1016/j.ccr.2021.213984.

2. J. D. Rinehart and J. R. Long, “Exploiting Single-Ion Anisotropy in the Design of f-Element Single-Molecule Magnets,” *Chemical Science* 2 (2011): 2078, https://doi.org/10.1039/c1sc00513h.

3. D. N. Woodruff, R. E. P. Winpenny, and R. A. Layfield, “Lanthanide Single-Molecule Magnets,” *Chemical Reviews* 113 (2013): 5110–5148, https://doi.org/10.1021/cr400018q.

4. T. G. Ashebr, H. Li, X. Ying, et al., “Emerging Trends on Designing High-Performance Dysprosium(III) Single-Molecule Magnets,” *ACS Materials Letters* 4 (2022): 307–319, https://doi.org/10.1021/acsmaterialslett.1c00765.

5. N. Ishikawa, M. Sugita, and W. Wernsdorfer, “Quantum Tunneling of Magnetization in Lanthanide Single-Molecule Magnets: Bis(Phthalocyaninato)Terbium and Bis(Phthalocyaninato)Dysprosium Anions,” *Angewandte Chemie International Edition* 44 (2005): 2931–2935, https://doi.org/10.1002/anie.200462638.

6. F. Ortu, D. Reta, Y.-S. Ding, et al., “Studies of Hysteresis and Quantum Tunnelling of the Magnetisation in Dysprosium(iii) Single Molecule Magnets,” *Dalton Transactions* 48 (2019): 8541–8545, https://doi.org/10.1039/C9DT01655D.

7. Y.-C. Chen and M.-L. Tong, “Single-Molecule Magnets Beyond a Single Lanthanide Ion: The Art of Coupling,” *Chemical Science* 13 (2022): 8716–8726, https://doi.org/10.1039/D2SC01532C.

8. F. Habib and M. Murugesu, “Lessons Learned From Dinuclear Lanthanide Nano-Magnets,” *Chemical Society Reviews* 42 (2013): 3278, https://doi.org/10.1039/c2cs35361j.

9. J. Tian, J. Du, B. Li, et al., “Recent Advances of Dinuclear Dysprosium-Based Single-Molecule Magnets: From Mechanisms to Application,” *Journal of Materials Chemistry C* 12 (2024): 14754–14773, https://doi.org/10.1039/D4TC01537A.

10. Q.-C. Luo, X.-L. Ding, W.-J. Xu, Y.-Q. Zhai, and Y.-Z. Zheng, “Equatorial Aminopyridine Ligands Stabilize an Unusual Straightly Bridging Mode in Dimeric Dysprosium(III) Single-Molecule Magnets,” *Chinese Chemical Letters* (2025): 110304, https://doi.org/10.1016/j.cclet.2024.110304.

11. P.-B. Jin, Q.-C. Luo, Y.-Y. Liu, and Y.-Z. Zheng, “Enhancing Blocking Temperature Using Inverse Hydrogen Bonds for Non-Radical Bridged Dimeric Dy(III) Single-Molecule Magnets,” *Science China Chemistry* 67 (2024): 3328–3338, https://doi.org/10.1007/s11426-024-2157-7.

12. Q.-C. Luo, K.-X. Yu, P.-B. Jin, Y.-Y. Liu, Y.-Q. Zhai, and Y.-Z. Zheng, “Strong Antiferromagnetic Exchange-Coupling Observed in Hydride-Bridged Dimeric Dysprosium(III) Single-Molecule Magnet,” *Chinese Journal of Chemistry* 42 (2024): 391–396, https://doi.org/10.1002/cjoc.202300491.

13. P.-B. Jin, Q.-C. Luo, Y.-Q. Zhai, et al., “A Study of Cation-Dependent Inverse Hydrogen Bonds and Magnetic Exchange-Couplings in Lanthanacarborane Complexes,” *Iscience* (2021): 102760, https://doi.org/10.1016/j.isci.2021.102760.

14. Y.-N. Guo, G.-F. Xu, W. Wernsdorfer, et al., “Strong Axiality and Ising Exchange Interaction Suppress Zero-Field Tunneling of Magnetization of an Asymmetric Dy$_2$ Single-Molecule Magnet,” *Journal of the American Chemical Society* 133 (2011): 11948–11951, https://doi.org/10.1021/ja205035g.

15. D.-D. Feng, F. Lu, Z.-Y. Liu, et al., “Side-Group Effect on the Slow Relaxations of {Dy$_2$ } Single-Molecule Magnets With Confined N$_2$ O$_6$ Donors,” *Inorganic Chemistry* 61 (2022): 13133–13142, https://doi.org/10.1021/acs.inorgchem.2c01865.

16. M.-X. Yao, Y.-Q. Gao, Z.-W. An, and D.-M. Zhu, “The Effect of Magnetic Coupling Along the Magnetic Axis on Slow Magnetic Relaxation in Dy^{III} Complexes With $_{5\ h}$ Configuration Based on an Aggregation-Induced-Emission-Active Ligand,” *Dalton Transactions* 53 (2024): 5133–5146, https://doi.org/10.1039/D3DT04257J.

17. Y. Peng, V. Mereacre, A. Baniodeh, et al., “Effect of Ligand Field Tuning on the SMM Behavior for Three Related Alkoxide-Bridged Dysprosium Dimers,” *Inorganic Chemistry* 55 (2016): 68–74, https://doi.org/10.1021/acs.inorgchem.5b01793.

18. P. Zhang, L. Zhang, S.-Y. Lin, S. Xue, and J. Tang, “Modulating Magnetic Dynamics of Dy$_2$ System Through the Coordination Geometry and Magnetic Interaction,” *Inorganic Chemistry* 52 (2013): 4587–4592, https://doi.org/10.1021/ic400150f.

19. P. Kumar, A. Swain, J. Acharya, et al., “Synthesis, Structure, and Zero-Field SMM Behavior of Homometallic Dy2, Dy4, and Dy6 Complexes,” *Inorganic Chemistry* 61 (2022): 11600–11621, https://doi.org/10.1021/acs.inorgchem.2c01041.

20. Y. Peng, V. Mereacre, C. E. Anson, et al., “Tuning of Hula-Hoop Coordination Geometry in a Dy Dimer,” *Inorganics* 4 (2016): 2.

21. L. Zou, L. Zhao, P. Chen, et al., “Phenoxido and Alkoxido-Bridged Dinuclear Dysprosium Complexes Showing Single-Molecule Magnet Behaviour,” *Dalton Transactions* 41 (2012): 2966, https://doi.org/10.1039/c2dt12235a.

22. K.-L. Zhong, X.-Q. Ma, Y.-H. Tong, et al., “Two Solvent-Stable Dy2 Compounds Constructed by a Large Conjugated Diacylhydrazone Ligand: Disparate Crystal Structures and Single-Molecule-Magnet Behaviors,” *Inorganica Chimica Acta* 557 (2023): 121702, https://doi.org/10.1016/j.ica.2023.121702.

23. M. Fondo, J. Corredoira-Vázquez, A. M. García-Deibe, et al., “Slow Magnetic Relaxation in Dinuclear Dysprosium and Holmium Phenoxide Bridged Complexes: A Dy$_2$ Single Molecule Magnet With a High Energy Barrier,” *Inorganic Chemistry Frontiers* 8 (2021): 2532–2541, https://doi.org/10.1039/D1QI00152C.

24. M. Kong, X. Feng, J. Wang, Y.-Q. Zhang, and Y. Song, “Tuning Magnetic Anisotropy via Terminal Ligands Along the Dy⋯Dy Orientation in Novel Centrosymmetric [Dy$_2$] Single Molecule Magnets,” *Dalton Transactions* 50 (2021): 568–577, https://doi.org/10.1039/D0DT03854G.

25. H.-S. Wang, P.-F. Zhou, J. Wang, et al., “Significantly Enhancing the Single-Molecule-Magnet Performance of a Dinuclear Dy(III) Complex by

Utilizing an Asymmetric Auxiliary Organic Ligand," *Inorganic Chemistry* 60 (2021): 18739–18752, https://doi.org/10.1021/acs.inorgchem.1c02169.

26. J. Long, F. Habib, P.-H. Lin, et al., "Single-Molecule Magnet Behavior for an Antiferromagnetically Superexchange-Coupled Dinuclear Dysprosium(III) Complex," *Journal of the American Chemical Society* 133 (2011): 5319–5328, https://doi.org/10.1021/ja109706y.

27. P. Lin, T. J. Burchell, R. Clérac, and M. Murugesu, "Dinuclear Dysprosium(III) Single-Molecule Magnets With a Large Anisotropic Barrier," *Angewandte Chemie International Edition* 47 (2008): 8848–8851, https://doi.org/10.1002/anie.200802966.

28. F. Habib, G. Brunet, V. Vieru, I. Korobkov, L. F. Chibotaru, and M. Murugesu, "Significant Enhancement of Energy Barriers in Dinuclear Dysprosium Single-Molecule Magnets Through Electron-Withdrawing Effects," *Journal of the American Chemical Society* 135 (2013): 13242–13245, https://doi.org/10.1021/ja404846s.

29. Y. Qin, H. Zhang, H. Sun, et al., "Two Series of Homodinuclear Lanthanide Complexes: Greatly Enhancing Energy Barriers through Tuning Terminal Solvent Ligands in Dy_2 Single-Molecule Magnets," *Chemistry—An Asian Journal* 12 (2017): 2834–2844, https://doi.org/10.1002/asia.201701065.

30. S. V. Klementyeva, M. T. Gamer, M. Schulze, et al., "Dinuclear Rare-Earth β-Diketiminates With Bridging 3,5-Di Tert -butyl-Catecholates: Synthesis, Structure, and Single-Molecule Magnet Properties," *Inorganic Chemistry* 64 (2025): 701–715, https://doi.org/10.1021/acs.inorgchem.4c03278.

31. S. Xue, Y. Guo, L. Ungur, J. Tang, and L. F. Chibotaru, "Tuning the Magnetic Interactions and Relaxation Dynamics of Dy_2 Single-Molecule Magnets," *Chemistry—A European Journal* 21 (2015): 14099–14106, https://doi.org/10.1002/chem.201501866.

32. H.-M. Dong, H.-Y. Li, Y.-Q. Zhang, E.-C. Yang, and X.-J. Zhao, "Magnetic Relaxation Dynamics of a Centrosymmetric Dy_2 Single-Molecule Magnet Triggered by Magnetic-Site Dilution and External Magnetic Field," *Inorganic Chemistry* 56 (2017): 5611–5622, https://doi.org/10.1021/acs.inorgchem.6b03089.

33. J. Wang, Q. Li, S. Wu, et al., "Opening Magnetic Hysteresis by Axial Ferromagnetic Coupling: From Mono-Decker to Double-Decker Metallacrown," *Angewandte Chemie International Edition* 60 (2021): 5299–5306, https://doi.org/10.1002/anie.202014993.

34. Z. Zhu, C. Zhao, Q. Zhou, et al., "Air-Stable Dy(III)-Macrocycle Enantiomers: From Chiral to Polar Space Group," *CCS Chemistry* 4 (2022): 3762–3771, https://doi.org/10.31635/ccschem.022.202101604.

35. C. Zhao, Z. Zhu, X.-L. Li, and J. Tang, "Air-Stable Chiral Mono- and Dinuclear Dysprosium Single-Molecule Magnets: Steric Hindrance of Hexaazamacrocycles," *Inorganic Chemistry Frontiers* 9 (2022): 4049–4055, https://doi.org/10.1039/D2QI00754A.

36. J. Xiong, H.-Y. Ding, Y.-S. Meng, et al., "Hydroxide-Bridged Five-Coordinate Dy^{III} Single-Molecule Magnet Exhibiting the Record Thermal Relaxation Barrier of Magnetization Among Lanthanide-Only Dimers," *Chemical Science* 8 (2017): 1288–1294, https://doi.org/10.1039/C6SC03621J.

37. J. D. Rinehart, M. Fang, W. J. Evans, and J. R. Long, "Strong Exchange and Magnetic Blocking in N23−-Radical-Bridged Lanthanide Complexes," *Nature Chemistry* 3 (2011): 538–542, https://doi.org/10.1038/nchem.1063.

38. S. Demir, M. I. Gonzalez, L. E. Darago, W. J. Evans, and J. R. Long, "Giant Coercivity and High Magnetic Blocking Temperatures for N_2^{3}– Radical-Bridged Dilanthanide Complexes Upon Ligand Dissociation," *Nature Communications* 8 (2017): 2144, https://doi.org/10.1038/s41467-017-01553-w.

39. C. A. Gould, E. Mu, V. Vieru, et al., "Substituent Effects on Exchange Coupling and Magnetic Relaxation in 2,2′-Bipyrimidine Radical-Bridged Dilanthanide Complexes," *Journal of the American Chemical Society* 142 (2020): 21197–21209, https://doi.org/10.1021/jacs.0c10612.

40. F. Benner, L. La Droitte, O. Cador, B. Le Guennic, and S. Demir, "Magnetic Hysteresis and Large Coercivity in Bisbenzimidazole Radical-Bridged Dilanthanide Complexes," *Chemical Science* 14 (2023): 5577–5592, https://doi.org/10.1039/D3SC01562A.

41. F. Benner and S. Demir, "From Unprecedented 2,2′-bisimidazole-Bridged Rare Earth Organometallics to Magnetic Hysteresis in the Dysprosium Congener," *Inorganic Chemistry Frontiers* 10 (2023): 4981–4992, https://doi.org/10.1039/D3QI00546A.

42. N. Mavragani, A. A. Kitos, R. Gayfullina, A. Mansikkamäki, J. O. Moilanen, and M. Murugesu, "Exploring the Substitution Effect on the Magnetic Coupling of Tetrazinyl-Bridged Ln_2 Single-Molecule Magnets," *Inorganic Chemistry Frontiers* 12 (2025): 3403–3415, https://doi.org/10.1039/D4QI02796E.

43. S. Demir, J. M. Zadrozny, M. Nippe, and J. R. Long, "Exchange Coupling and Magnetic Blocking in Bipyrimidyl Radical-Bridged Dilanthanide Complexes," *Journal of the American Chemical Society* 134 (2012): 18546–18549, https://doi.org/10.1021/ja308945d.

44. F. Benner, S. Deshapriya, and S. Demir, "A Tetraazanaphthalene Radical-Bridged Dysprosium Single-Molecule Magnet With a Large Coercive Field," *Chemical Science* 16 (2025): 20806–20822, https://doi.org/10.1039/D5SC05358G.

45. F. Benner, S. Deshapriya, J. Hrubý, S. Hill, and S. Demir, "Magnetic Blocking in Fluoflavine Radical-Bridged Dilanthanide Complexes," *Journal of the American Chemical Society* 147 (2025): 47159–47178, https://doi.org/10.1021/jacs.5c14158.

46. H. Wu, M. Li, Z. Xia, et al., "High Temperature Quantum Tunnelling of Magnetization and Thousand Kelvin Anisotropy Barrier in a Dy_2 Single-Molecule Magnet," *Chemical Communications* 57 (2021): 371–374, https://doi.org/10.1039/D0CC06993K.

47. T. Han, M. J. Giansiracusa, Z. Li, et al., "Exchange-Biasing in a Dinuclear Dysprosium(III) Single-Molecule Magnet With a Large Energy Barrier for Magnetisation Reversal," *Chemistry—A European Journal* 26 (2020): 6773–6777, https://doi.org/10.1002/chem.202000719.

48. T. Han, Y.-S. Ding, Z.-H. Li, et al., "A Dichlorido-Bridged Dinuclear Dy(iii) Single-Molecule Magnet With an Effective Energy Barrier Larger Than 600 K," *Chemical Communications* 55 (2019): 7930–7933, https://doi.org/10.1039/C9CC02436K.

49. M. Li, H. Wu, Z. Xia, et al., "Bromine-Bridged Dy_2 Single-Molecule Magnet: Magnetic Anisotropy Driven by Cis / Trans Stereoisomers," *Chemical Communications* 55 (2019): 14661–14664, https://doi.org/10.1039/C9CC07552F.

50. C. A. Gould, K. R. McClain, D. Reta, et al., "Ultrahard Magnetism From Mixed-Valence Dilanthanide Complexes With Metal-Metal Bonding," *Science* 375 (2022): 198–202, https://doi.org/10.1126/science.abl5470.

51. L. Zhang, H. Ma, Z.-Q. Wang, Y.-M. Tian, Y.-Q. Zhang, and W.-B. Sun, "Double and triple pyridine-N-oxide bridged dinuclear Dysprosium(III) dimers and single-molecule magnetic properties," *Journal of Molecular Structure* 1175 (2019): 686–697.

52. X. Yi, F. Pointillart, B. Le Guennic, et al., "Rational Engineering of Dimeric Dy-Based Single-Molecule Magnets for Surface Grafting," *Polyhedron* 164 (2019): 41–47, https://doi.org/10.1016/j.poly.2019.02.040.

53. I. Cimatti, X. Yi, R. Sessoli, et al., "Chemical Tailoring of Single Molecule Magnet Behavior in Films of Dy(III) Dimers," *Applied Surface Science* 432 (2018): 7–14, https://doi.org/10.1016/j.apsusc.2017.06.024.

54. T. Han, W. Shi, X.-P. Zhang, L.-L. Li, and P. Cheng, "A Family of Binuclear Dysprosium(III) Radical Compounds With Magnetic Relaxation in ON and OFF States," *Inorganic Chemistry* 51 (2012): 13009–13016, https://doi.org/10.1021/ic3021244.

55. S. K. Kuppusamy, E. Moreno-Pineda, A. M. Nonat, et al., "Binuclear Lanthanide Complexes Based on 4-Picoline- N -Oxide: From Sensitized Luminescence to Single-Molecule Magnet Characteristics," *Crystal Growth & Design* 23 (2023): 1084–1094, https://doi.org/10.1021/acs.cgd.2c01234.

56. F. Pointillart, B. Le Guennic, S. Golhen, O. Cador, and L. Ouahab, "Slow Magnetic Relaxation in Radical Cation Tetrathiafulvalene-Based

Lanthanide(iii) Dinuclear Complexes," *Chemical Communications* 49 (2013): 11632, https://doi.org/10.1039/c3cc47087c.

57. K. Murashima, S. Karasawa, K. Yoza, Y. Inagaki, and N. Koga, "3- and 4-(α-Diazobenzyl)Pyridine-N-Oxides as Photoresponsive Magnetic Couplers for 2p–4f Heterospin Systems: Formation of Carbene–Tb$^{\text{III}}$ and Carbene–Dy$^{\text{III}}$ Single-Molecule Magnets," *Dalton Transactions* 45 (2016): 7067–7077, https://doi.org/10.1039/C6DT00420B.

58. J. Wang, M. Yang, J. Sun, et al., "Enhancing the Energy Barrier of Dysprosium(iii) Single-Molecule Magnets by Tuning the Magnetic Interactions Through Different N -Oxide Bridging Ligands," *CrystEngComm* 21 (2019): 6219–6225, https://doi.org/10.1039/C9CE01378D.

59. F. Pointillart, Y. Le Gal, S. Golhen, O. Cador, and L. Ouahab, "Single-Molecule Magnet Behaviour in a Tetrathiafulvalene-Based Electroactive Antiferromagnetically Coupled Dinuclear Dysprosium(III) Complex," *Chemistry—A European Journal* 17 (2011): 10397–10404, https://doi.org/10.1002/chem.201100869.

60. H. Douib, B. Lefeuvre, K. Dhbaibi, J. Flores Gonzalez, V. Dorcet, and F. Pointillart, "Molecular Architecture and Single-Molecule Magnet Behavior Control by Playing With Lanthanide Ionic Radii and Bulkiness Ancillary Ligands," *Chemistry—An Asian Journal* 20 (2025): e202500234, https://doi.org/10.1002/asia.202500234.

61. X. Yi, K. Bernot, F. Pointillart, et al., "A Luminescent and Sublimable Dy$^{\text{III}}$ -Based Single-Molecule Magnet," *Chemistry—A European Journal* 18 (2012): 11379–11387, https://doi.org/10.1002/chem.201201167.

62. D. Shao, P. P. Sahu, W.-J. Tang, et al., "A Single-Ion Magnet Building Block Strategy Toward dy$_2$ Single-Molecule Magnets With Enhanced Magnetic Performance," *Dalton Transactions* 51 (2022): 18610–18621, https://doi.org/10.1039/D2DT03046B.

63. H. Douib, K. Dhbaibi, B. Lefeuvre, V. Dorcet, T. Guizouarn, and F. Pointillart, "Bulky Anion Effect on the Architecture of Chiral Dysprosium Single-Molecule Magnets," *Chirality* 35 (2023): 155–164, https://doi.org/10.1002/chir.23528.

64. H. Douib, B. Lefeuvre, J. Flores Gonzalez, V. Dorcet, and F. Pointillart, "Versatility of the Methyl-Bipyrimidine- N -Oxide Ligand for the Design of Lanthanide Single-Molecule Magnets," *CrystEngComm* 27 (2025): 7677–7688, https://doi.org/10.1039/D5CE00831J.

65. G. Huang, X. Yi, J. Jung, et al., "Optimization of Magnetic Relaxation and Isotopic Enrichment in Dimeric Dy$^{\text{III}}$ Single-Molecule Magnets," *European Journal of Inorganic Chemistry* 2018 (2018): 326–332, https://doi.org/10.1002/ejic.201700842.

66. L. Zhang, P. Chen, H. Li, Y. Tian, P. Yan, and W. Sun, "Structure and Single-Molecule Magnetic Property of a Dinuclear Dy$_2$ Complex Bridged by the 4-Methylpyridine N -Oxide Ligand," *European Journal of Inorganic Chemistry* 2018 (2018): 3668–3674, https://doi.org/10.1002/ejic.201800596.

67. X. Wang, M. Zhou, W. Wang, et al., "Enhancing the Magnetic Behaviors of Dy2 Complexes by Modulating the Crystal Field Environment With Different μ-O Bridging Ligands," *Molecules (Basel, Switzerland)* 30 (2025): 1260, https://doi.org/10.3390/molecules30061260.

68. X. Yi, G. Calvez, C. Daiguebonne, O. Guillou, and K. Bernot, "Rational Organization of Lanthanide-Based SMM Dimers Into Three-Dimensional Networks," *Inorganic Chemistry* 54 (2015): 5213–5219, https://doi.org/10.1021/acs.inorgchem.5b00087.

69. X. Yi, J. Shang, L. Pan, et al., "Reversible Luminescence Modulation Upon an Electric Field on a Full Solid-State Device Based on Lanthanide Dimers," *ACS Applied Materials & Interfaces* 8 (2016): 15551–15556, https://doi.org/10.1021/acsami.6b04451.

70. K. Bernot, C. Daiguebonne, G. Calvez, Y. Suffren, and O. Guillou, "A Journey in Lanthanide Coordination Chemistry: From Evaporable Dimers to Magnetic Materials and Luminescent Devices," *Accounts of Chemical Research* 54 (2021): 427–440, https://doi.org/10.1021/acs.accounts.0c00684.

71. E. Kiefl, M. Mannini, K. Bernot, et al., "Robust Magnetic Properties of a Sublimable Single-Molecule Magnet," *ACS Nano* 10 (2016): 5663–5669, https://doi.org/10.1021/acsnano.6b01817.

72. O. Sun, P. Chen, H.-F. Li, T. Gao, and P.-F. Yan, "Structural, Photophysical and Magnetic Studies of {Ln$_2$} Assembled About Oxime," *Inorganic Chemistry Communications* 114 (2020): 107841, https://doi.org/10.1016/j.inoche.2020.107841.

73. L. Yang, Y. Zhang, L. Hu, et al., "Synthesis, Characterization and Cell Imaging Properties of Rare Earth Compounds Based on Hydroxamate Ligand," *Journal of Rare Earths* 36 (2018): 418–423, https://doi.org/10.1016/j.jre.2017.11.004.

74. A. S. Armenis, D. I. Alexandropoulos, A. Worrell, L. Cunha-Silva, K. R. Dunbar, and T. C. Stamatatos, "Peripheral Site Modification in a Family of Dinuclear [Dy$_2$ (hynad)$_{2–6}$ (NO$_3$)$_{0–6}$ (sol)$_{0–2}$]$^{0/2−}$ Single-Molecule Magnets Bearing a {Dy$_2$ (μ-OR)$_2$ }$^{4+}$ Diamond-Shaped Core and Exhibiting Dissimilar Magnetic Dynamics," *Dalton Transactions* 52 (2023): 13565–13577, https://doi.org/10.1039/D3DT02596A.

75. A. S. Armenis, A. Worrell, D. I. Alexandropoulos, J. Tang, and T. C. Stamatatos, "A Leap Forward in the Coordination Chemistry of N -Hydroxy-1,8-Naphthalimide Chelate: New {Dy$_2$ } and {Dy$_5$ } Single-Molecule Magnets and the Structure-Directing Role of Supporting β-Diketonate Ligands," *Crystal Growth & Design* 24 (2024): 9243–9253, https://doi.org/10.1021/acs.cgd.4c01229.

76. E. C. Mazarakioti, J. Regier, L. Cunha-Silva, et al., "Large Energy Barrier and Magnetization Hysteresis at 5 K for a Symmetric {Dy$_2$ } Complex With Spherical Tricapped Trigonal Prismatic Dy$^{\text{III}}$ Ions," *Inorganic Chemistry* 56 (2017): 3568–3578, https://doi.org/10.1021/acs.inorgchem.7b00026.

77. S. T. Liddle and J. Van Slageren, "Improving f-Element Single Molecule Magnets," *Chemical Society Reviews* 44 (2015): 6655–6669, https://doi.org/10.1039/C5CS00222B.

78. R. J. Blagg, L. Ungur, F. Tuna, et al., "Magnetic Relaxation Pathways in Lanthanide Single-Molecule Magnets," *Nature Chemistry* 5 (2013): 673–678, https://doi.org/10.1038/nchem.1707.

79. A. Lunghi, F. Totti, R. Sessoli, and S. Sanvito, "The Role of Anharmonic Phonons in Under-Barrier Spin Relaxation of Single Molecule Magnets," *Nature Communications* 8 (2017): 14620, https://doi.org/10.1038/ncomms14620.

80. E. Garlatti, A. Albino, S. Chicco, et al., "The Critical Role of Ultra-Low-Energy Vibrations in the Relaxation Dynamics of Molecular Qubits," *Nature Communications* 14 (2023): 1653, https://doi.org/10.1038/s41467-023-36852-y.

81. E. Garlatti, A. Chiesa, P. Bonfà, et al., "A Cost-Effective Semi-Ab Initio Approach to Model Relaxation in Rare-Earth Single-Molecule Magnets," *Journal of Physical Chemistry Letters* 12 (2021): 8826–8832, https://doi.org/10.1021/acs.jpclett.1c02367.

82. W. Wernsdorfer, N. E. Chakov, and G. Christou, "Determination of the Magnetic Anisotropy Axes of Single-Molecule Magnets," *Physical Review B* 70 (2004): 132413, https://doi.org/10.1103/PhysRevB.70.132413.

83. A. B. Carter, J. Braun, T. Bodenstein, et al., "Using a Radical Straitjacket to Enforce an Ultrashort Dy–Dy Distance and Thus Enhance Dipolar Interactions in a Dy$^{\text{II}}_2$ Dimer," *Inorganic Chemistry* 64 (2025): 25036–25043, https://doi.org/10.1021/acs.inorgchem.5c04406.

84. C. Uhlmann, L. Münzfeld, A. Hauser, et al., "Unique Double and Triple Decker Arrangements of Rare-Earth 9,10-Diborataanthracene Complexes Featuring Single-Molecule Magnet Characteristics," *Angewandte Chemie International Edition* 63 (2024): e202401372, https://doi.org/10.1002/anie.202401372.

85. C. Y. Chow, H. Bolvin, V. E. Campbell, et al., "Assessing the Exchange Coupling in Binuclear Lanthanide(iii) Complexes and the Slow Relaxation of the Magnetization in the Antiferromagnetically Coupled Dy$_2$ Derivative," *Chemical Science* 6 (2015): 4148–4159, https://doi.org/10.1039/C5SC01029B.

86. E. Moreno-Pineda, G. Taran, W. Wernsdorfer, and M. Ruben, "Quantum Tunnelling of the Magnetisation in Single-Molecule Magnet Isotopologue Dimers," *Chemical Science* 10 (2019): 5138–5145, https://doi.org/10.1039/C9SC01062A.

87. E. M. Pineda, Y. Lan, O. Fuhr, W. Wernsdorfer, and M. Ruben, "Exchange-Bias Quantum Tunnelling in a CO_2 -Based Dy_4 -Single Molecule Magnet," *Chemical Science* 8 (2017): 1178–1185, https://doi.org/10.1039/C6SC03184F.

88. N. F. Chilton, D. Collison, E. J. L. McInnes, R. E. P. Winpenny, and A. Soncini, "An Electrostatic Model for the Determination of Magnetic Anisotropy in Dysprosium Complexes," *Nature Communications* 4 (2013): 2551, https://doi.org/10.1038/ncomms3551.

89. M. E. Lines, "Orbital Angular Momentum in the Theory of Paramagnetic Clusters," *Journal of Chemical Physics* 55 (1971): 2977–2984, https://doi.org/10.1063/1.1676524.

90. N. F. Chilton, R. P. Anderson, L. D. Turner, A. Soncini, and K. S. Murray, "PHI: A Powerful New Program for the Analysis of Anisotropic Monomeric and Exchange-Coupled Polynuclear D - and f -Block Complexes," *Journal of Computational Chemistry* 34 (2013): 1164–1175, https://doi.org/10.1002/jcc.23234.

91. Y.-S. Meng, S.-D. Jiang, B.-W. Wang, and S. Gao, "Understanding the Magnetic Anisotropy Toward Single-Ion Magnets," *Accounts of Chemical Research* 49 (2016): 2381–2389, https://doi.org/10.1021/acs.accounts.6b00222.

92. P. Loeffen, *Oxford Diffraction CrysAlis CCD and CrysAlis RED* (Oxford Diffraction Ltd., 2008).

93. A. Altomare, G. Cascarano, C. Giacovazzo, et al., "SIRPOW.92 - a program for automatic solution of crystal structures by direct methods optimized for powder data," *Journal of Applied Crystallography* 27 (1994): 435.

94. G. M. Sheldrick, *SHELXS-97 and SHELXL-97, Program for Crystal Structure Solution and Refinement* (University of Gottingen, 1997).

95. G. M. Sheldrick, "Crystal Structure Refinement With SHELXL," *Acta Crystallographica Section C Structural Chemistry* 71 (2015): 3–8, https://doi.org/10.1107/S2053229614024218.

96. G. M. Sheldrick, "SHELXT—Integrated Space-Group and Crystal-Structure Determination," *Acta Crystallographica Section A Foundations and Advances* 71 (2015): 3–8, https://doi.org/10.1107/S2053273314026370.

97. L. J. Farrugia, "WinGX Suite for Small-Molecule Single-Crystal Crystallography," *Journal of Applied Crystallography* 32 (1999): 837–838, https://doi.org/10.1107/S0021889899006020.

98. C. F. Macrae, P. R. Edgington, P. McCabe, et al., "Mercury: Visualization and Analysis of Crystal Structures," *Journal of Applied Crystallography* 39 (2006): 453–457, https://doi.org/10.1107/S002188980600731X.

99. Crystal Impact GbR, K. Brandenburg and H. Putz, DIAMOND, Release 3.1f, (2006).

100. G. A. Bain and J. F. Berry, "Diamagnetic Corrections and Pascal's Constants," *Journal of Chemical Education* 85 (2008): 532, https://doi.org/10.1021/ed085p532.

101. W. Wernsdorfer, "Classical and Quantum Magnetization Reversal Studied in Nanometer-Sized Particles and Clusters," *Advances in Chemical Physics* 118 (2001): 99–190, https://doi.org/10.1002/9780470141786.ch3.

102. G. Li Manni, I. F. Galván, A. Alavi, et al., "The OpenMolcas Web: A Community-Driven Approach to Advancing Computational Chemistry," *Journal of Chemical Theory and Computation* 19 (2023): 6933–6991, https://doi.org/10.1021/acs.jctc.3c00182.

103. F. Aquilante, J. Autschbach, R. K. Carlson, et al., "Molcas 8: New Capabilities for Multiconfigurational Quantum Chemical Calculations across the Periodic Table," *Journal of Computational Chemistry* 37 (2016): 506–541, https://doi.org/10.1002/jcc.24221.

104. J. Olsen, B. O. Roos, P. Jo/rgensen, and H. J. A. Jensen, "Determinant Based Configuration Interaction Algorithms for Complete and Restricted Configuration Interaction Spaces," *Journal of Chemical Physics* 89 (1988): 2185–2192, https://doi.org/10.1063/1.455063.

105. P. E. M. Siegbahn, J. Almlöf, A. Heiberg, and B. O. Roos, "The Complete Active Space SCF (CASSCF) Method in a Newton–Raphson Formulation with Application to the HNO Molecule," *Journal of Chemical Physics* 74 (1981): 2384–2396, https://doi.org/10.1063/1.441359.

106. B. Roos, R. Lindh, P.-Å. Malmqvist, V. Veryazov, and P.-O. Widmark, "Main Group Atoms and Dimers Studied With a New Relativistic ANO Basis Set," *Journal of Physical Chemistry A* 108 (2004): 2851–2858, https://doi.org/10.1021/jp031064+.

107. B. O. Roos, R. Lindh, P.-Å. Malmqvist, V. Veryazov, P.-O. Widmark, and A. C. Borin, "New Relativistic Atomic Natural Orbital Basis Sets for Lanthanide Atoms With Applications to the Ce Diatom and LuF_3," *Journal of Physical Chemistry A* 112 (2008): 11431–11435, https://doi.org/10.1021/jp803213j.

108. P.-O. Widmark, P.-Å. Malmqvist, and B. O. Roos, "Density Matrix Averaged Atomic Natural Orbital (ANO) Basis Sets for Correlated Molecular Wave Functions," *Theoretica Chimica Acta* 77 (1990): 291–306, https://doi.org/10.1007/BF01120130.

109. D. Peng and K. Hirao, "An Arbitrary Order Douglas–Kroll Method With Polynomial Cost," *Journal of Chemical Physics* 130 (2009): 044102, https://doi.org/10.1063/1.3068310.

110. P. Å. Malmqvist, B. O. Roos, and B. Schimmelpfennig, "The Restricted Active Space (RAS) State Interaction Approach With Spin–Orbit Coupling," *Chemical Physics Letters* 357 (2002): 230–240, https://doi.org/10.1016/S0009-2614(02)00498-0.

111. L. Ungur and L. F. Chibotaru, "Ab Initio Crystal Field for Lanthanides," *Chemistry—A European Journal* 23 (2017): 3708–3718, https://doi.org/10.1002/chem.201605102.

112. L. F. Chibotaru and L. Ungur, "Ab Initio Calculation of Anisotropic Magnetic Properties of Complexes. I. Unique Definition of Pseudospin Hamiltonians and Their Derivation," *Journal of Chemical Physics* 137 (2012): 064112, https://doi.org/10.1063/1.4739763.

Supporting Information

Additional supporting information can be found online in the Supporting Information section.

Supporting File: chem70936-sup-0001-SuppMat.docx.